Transverse jet lock-in and quasiperiodicity

Takeshi Shoji, Elijah W. Harris, Andrea Besnard, Stephen G. Schein, and Ann R. Karagozian*

Department of Mechanical and Aerospace Engineering, University of California, Los Angeles, Los Angeles, California 90095, USA

(Received 10 July 2019; published 7 January 2020)

This experimental study explored the dynamics of lock-in phenomena associated with upstream shear layer (USL) instabilities for an equidensity gaseous jet in crossflow (JICF). Axisymmetric sinusoidal forcing of the jet fluid at different forcing amplitudes and frequencies was used to explore lock-in under flow conditions corresponding to naturally occurring absolutely/globally unstable and convectively/locally unstable shear layers, at relatively low and high jet-to-crossflow momentum flux ratios J, respectively. Dynamical phenomena were quantified via hotwire anemometry, which not only documented differences in spectral characteristics but also in Poincaré maps obtained via time-delay embedding in the temporal data. The experiments provided evidence of unconditional lock-in as well as quasiperiodicity in response to forcing, reflective of marginal lock-in phenomena; these phenomena were observed for both globally unstable and convectively/locally unstable shear layers in the absence of forcing. The free jet limit in the absence of crossflow also exhibited unconditional lock-in, with some characteristics similar to those for the JICF at applied forcing frequencies above the fundamental mode. For the globally unstable JICF, a simple van der Pol nonlinear oscillator model used to represent the dynamics of the USL showed consistency with experimental findings and thus provided additional insights into the nature of shear layer dynamics.

DOI: 10.1103/PhysRevFluids.5.013901

I. INTRODUCTION

The canonical jet in crossflow (JICF) or transverse jet typically consists of a round jet issuing perpendicularly into crossflow [1–3], generating diverse vortical structures as shown schematically in Fig. 1. Here the jet has a mean velocity of U_j at the exit plane, exhausting into crossflow with a freestream velocity U_∞ (outside of the injection wall boundary layer) in the positive x direction. The trajectory of the transverse jet's upstream shear layer (USL) is parameterized by the coordinate s. Commonly used nondimensional parameters used to characterize JICF behavior include the jet-to-crossflow density ratio, $S = \rho_j/\rho_\infty$, velocity ratio, $R = U_j/U_\infty$, and momentum flux ratio, $J \equiv \rho_j U_j^2/\rho_\infty U_\infty^2 = SR^2$ [4]. The Reynolds number of the jet, $\mathrm{Re}_j = \rho_j U_j D/\mu_j$, is based on jet diameter, D, and jet dynamic viscosity μ_j.

Of the vortical structures shown for the flush-injected JICF, the counter-rotating vortex pair (CVP) has long been understood to dominate the transverse jet's cross-section [4–7] and is thought to enhance the entrainment of crossflow into the jet in comparison to that for the free jet in quiescent surroundings. Experimental and computational studies demonstrate the relevance

*ark@seas.ucla.edu

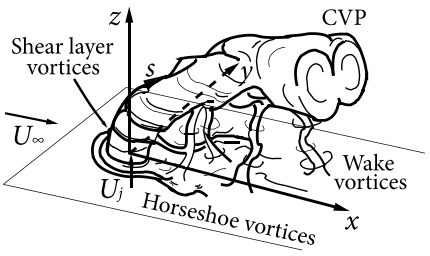

FIG. 1. Schematic of the transverse jet, introduced flush with respect to the injection wall, and relevant vortical structures, including the counter-rotating vortex pair (CVP). Here (x, y, z) refer to the jet coordinate system, and s refers to the upstream shear layer trajectory coordinate. Adapted from Fric and Roshko [9].

of the transverse jet's upstream shear layer vorticity to the formation and evolution of the CVP [6–8].

A. Unforced JICF instability, structures, and mixing

Experimental studies on the gaseous JICF have focused on upstream shear layer (USL) stability and structural characteristics for a range of flow conditions [8,10–12] in addition to explorations of JICF molecular mixing characteristics [13] and strain/scalar dissipation rate fields [14], all in the absence of any significant external jet excitation. Using hotwire anemometry, Megerian *et al.* [10] and Davitian *et al.* [11] experimentally investigate the stability characteristics of the equidensity ($S = 1$) transverse jet's USL at $\mathrm{Re}_j = 2000$ and 3000 for velocity ratios in the range $1.15 \leqslant R \leqslant \infty$, with a nitrogen jet injected flush into a crossflow of air. The studies demonstrate the transition from a convectively unstable (CU) USL, for which the instability evolves along the shear layer, to an absolutely unstable (AU) or globally unstable (GU) USL, with sustained self-excited global oscillations affecting the entire flowfield. Such instabilities transition as one increases the crossflow velocity, reducing R or J, for a fixed Re_j. For the nitrogen jet injected into a crossflow of air, the transition from CU to GU occurs at approximately $R = 3.1$ ($J \approx 10$). For separate experiments on the low density JICF, with $0.25 \leqslant S \leqslant 1.00$ achieved by using mixtures of helium and nitrogen in the jet fluid, the transition to absolute instability is documented in Getsinger *et al.* [12] to occur in the range of either $J \cong 10$ or $S \lesssim 0.40$ (at $\mathrm{Re}_j \cong 1800$). Evidence for this transition for both equidensity and low density transverse jets includes quantification of the growth of disturbances at various locations along the jet shear layer, frequency tracking and response of the transverse jet to very strong single-mode forcing, creating a lock-in response in the shear layer, and evidence of USL dynamics suggesting a Hopf bifurcation to a global mode. Direct numerical simulation (DNS) of the JICF at $R = 4$ and 2 by Iyer and Mahesh [15], with geometry and inlet flow conditions identical to those in Megerian *et al.* [10], show USL spectral characteristics that are qualitatively and quantitatively in good agreement with experiments, including differences in the spectral character for these conditions straddling the CU to AU transition.

Recent experiments utilizing optical diagnostics (acetone planar laser-induced fluorescence or PLIF imaging and stereo particle image velocimetry or PIV) enable investigation of JICF structural as well as mixing and strain field characteristics [8,13,14]. For the flush nozzle-injected JICF, the formation of the rolled-up vortical structures on the USL occurs closer to the jet exit as J decreases, especially for $J \lesssim 10$, as expected per spectral characteristics. Transverse jets at these lower J values produce a highly symmetric CVP in the cross-sectional view of the JICF. But interestingly, at higher J values where the USL is CU, asymmetric cross-sections are observed, for example, for $J > 20$. A more symmetric cross-section for the JICF is associated with improved molecular mixing [13], and jet excitation can be used to alter jet structure, documented to improve mixing [16,17]. Hence, the dynamics of the jet's upstream shear layer, and the ability to control it via excitation, is of interest for many applications.

B. Lock-in and quasiperiodicity

External periodic excitation of a jet in quiescent surroundings [18] or issuing into crossflow [10,19–22] is known to have the ability to change the dynamics and structural characteristics of the jet, potentially creating an enhancement in molecular mixing. In general, axisymmetric sinusoidal excitation of a flowfield is associated with interactions between a natural or fundamental mode of the flow in the absence of forcing and the forcing mode itself, potentially causing the flow to be marginally or fully locked-in to the applied forcing frequency and overcoming the natural mode. This phenomenon is known as "lock-in," the dynamical characteristics of which are significant in achieving optimized control of a flowfield (e.g., improving molecular mixing) via external forcing.

Lock-in has been observed for a number of unsteady flowfields, for example for vortex shedding in the wake of a vibrating circular cylinder [23–26]. The cylinder's natural vortex shedding frequency in the absence of forcing, f_o, can become locked-in, or synchronized, to the cylinder's forced vibrational frequency, f_f, over a specific range of forcing frequencies and amplitudes, creating a so-called a lock-in band [27]. Outside of this band of forcing conditions, the natural frequency f_o dominates the shedding phenomena. The Reynolds numbers explored for wake lock-in (Re $\approx$ 100–9200) are such that in all cases the cylinder wake is AU when unforced [28,29]. Lock-in phenomena are associated with other self-excited flows, including low density and reactive free jets in quiescent surroundings [30–32]. For example, Juniper *et al.* [30] explore lock-in for a nonreacting helium free jet and buoyant reactive jet diffusion flame under absolutely unstable flow conditions, with imposed axisymmetric sinusoidal jet forcing. They demonstrate that there is a critical range of excitation amplitudes and frequencies at which the global mode of the jet at its natural frequency f_o (in the absence of forcing) disappears and the forced mode with frequency f_f becomes dominant in shear layer spectra. Juniper *et al.* [30] thus create a "lock-in" diagram over a range of frequencies (f_f/f_o values) and amplitudes (e.g., input voltage to a speaker) at which lock-in occurs. The lock-in diagram (amplitude vs. forcing frequency or f_f/f_o at lock-in) typically takes a V-shape with respect to $f_f/f_o = 1$ because of the linear relationship between critical input voltages and $|f_f - f_o|$, although there can be asymmetric skewing of the V-shape due to differing shear layer responses at higher as compared with lower forcing frequencies [31]. Li and Juniper [31] actually find several kinds of of nonlinear dynamics for various combinations of f_f and amplitude, including: (1) cases where the natural frequency, f_o, or one slightly shifted from f_o, can dominate during very low amplitude forcing, (2) cases where "quasiperiodicity" can occur, where linear combinations of the forcing frequency f_f and f_o can appear in spectra during intermediate amplitude forcing, and (3) cases where "1:1 lock-in" occurs, in which the forcing frequency f_f itself dominates and f_o is significantly diminished during excitation at a fairly high amplitude.

Lock-in behavior for the upstream shear layer has been identified for both equidensity and low density jets in crossflow. For a relatively limited set of hotwire-acquired data, Davitian *et al.* [11] explore the effect of sinusoidal excitation for the equidensity nitrogen (N_2) jet issuing into a crossflow of air, documenting a lock-in type of response of the globally unstable USL for forcing frequencies close to the fundamental unforced value (f_o) or at high enough amplitudes of excitation, where amplitude is defined in terms of the jet velocity perturbation near the jet exit. A slight asymmetry in the lock-in diagram suggests that the USL is more resistant to lower frequency excitation ($f_f < f_o$) than to higher frequency excitation ($f_f > f_o$), requiring higher amplitude forcing to achieve lock-in at lower frequencies. In these equidensity JICF studies, the convectively unstable USL is suggested to be always (unconditionally) locked-in under axisymmetric sine wave forcing, even at very low amplitudes, although there are limited datasets at very low frequency forcing conditions. In contrast, the transverse jet's globally/absolutely unstable USL locks in only within a lock-in band (i.e., is conditionally locked-in). For low density jets in crossflow, Getsinger *et al.* [12] explore lock-in via sinusoidal excitation of a gaseous jet consisting of mixtures of nitrogen and helium injected into a crossflow of air, hence enabling variable S and J conditions. A conditional lock-in response of the jet's USL to sinusoidal forcing is observed for a range of frequencies and amplitudes (here, quantified in terms of acoustic pressure perturbation). An asymmetry in the lock-in

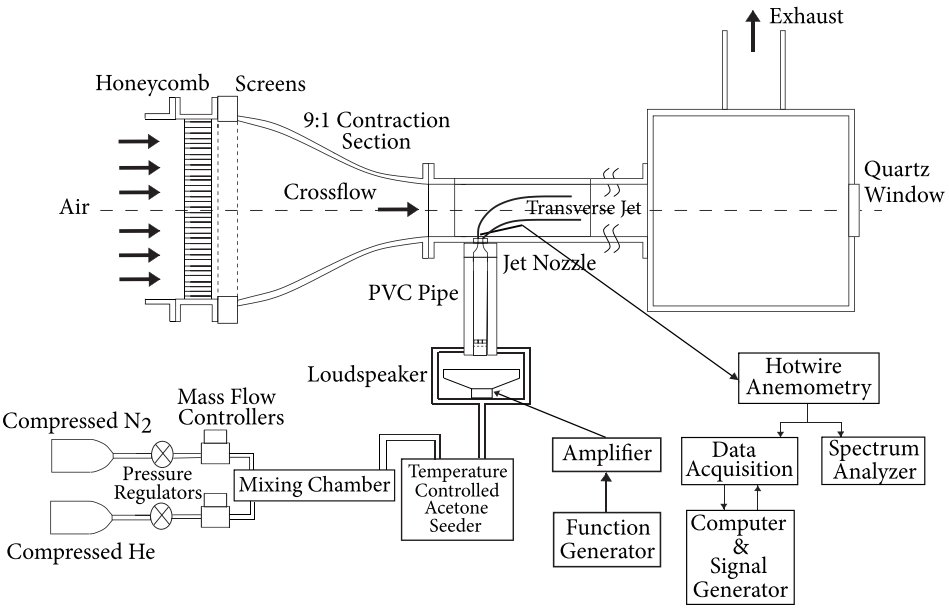

FIG. 2. Variable density transverse jet wind tunnel with associated hotwire anemometry and data acquisition. One additional tunnel section, of identical dimensions, was situated downstream of the test section shown.

diagram for GU/AU conditions with $S = 0.55$ and $J = 5$, for example, suggests that the USL with a higher forcing frequency ($f_f > f_o$) has a greater resistance to lock-in than forcing at lower frequencies $f_f < f_o$), consistent with findings of Li and Juniper [31] for a low density free jet. Other lock-in diagrams for the JICF with $S = 0.55$ and $J = 8$ and 10 are relatively symmetric, however, suggesting potential differences in dynamic response when crossflow conditions are altered.

The goal of the present equidensity JICF experiments is to explore the dynamics of lock-in for the USL in greater depth, not only as a means of understanding the similarities/differences with respect to other globally unstable flows, but also to inform transverse jet control strategies. The range of flow conditions here spanned both globally/absolutely unstable jet shear layers as well as locally/convectively unstable upstream shear layers. Detailed examination of and evidence for the phenomena of quasiperiodicity and 1:1 lock-in, and representation using a simple nonlinear Van der Pol oscillator model [31], provide new insights for the mechanisms of shear layer transition in the JICF and means by which it may be controlled.

II. EXPERIMENTAL CONFIGURATION

This experimental study utilized a low-velocity wind tunnel to measure gaseous transverse jet upstream shear layer stability characteristics, as done in prior studies [10–12]. A schematic of the wind tunnel and associated diagnostics is shown in Fig. 2. A centrifugal blower Baldor M3546-T) upstream of the test section created a crossflow of air in the downstream (positive x) direction with freestream velocity, U_∞, calibrated in the tunnel using a pitot probe. The flow from the blower issued into the test section through a 9:1 area ratio contraction section with honeycomb and screens for flow straightening. The maximum achievable flow velocity in the test section was approximately 7 m/s, with a maximum turbulence intensity was less than 1.5% in the freestream. The primary test section was 30 cm × 12 cm × 12 cm, fitted flush with the contraction section, and with quartz windows at the top for laser sheet access and plexiglass side windows for camera imaging in PLIF or PIV diagnostics [8,13,14]. A black panel with a cut-out could replace one of the side plexiglass windows to enable access for hotwire anemometry and the traversing mechanism. Another tunnel

section with the same size was placed downstream of the primary one; this section was followed by a wooden chamber which exhausted the gases via a flexible tube connected to the ventilation system of the laboratory.

Jet fluid issued perpendicularly into the test section through a contoured nozzle with a fifth-order polynomial contraction, with an exit plane inner diameter 4.04 mm. This contraction created a top-hat-like spatial velocity profile at the exit of the jet, with a fairly thin jet boundary layer in the absence of crossflow [10]. The injector exit was mounted flush to the primary test section's floor at a location 10 cm downstream of the end of the tunnel contraction. A longitudinal straight PVC pipe of length 0.9 m was attached to the bottom of the injector to eliminate swirl or other asymmetries via internal honeycomb flow straighteners. The other end of the PVC pipe was connected to the jet excitation system.

An acoustic loudspeaker (RadioShack 40-1022B, 4″ woofer) was situated below the pipe (see Fig. 2), introducing a sinusoidal oscillation in the jet fluid over time. The speaker was enclosed by a plexiglass plenum housing attached to the bottom of the PVC pipe, even for unforced transverse jet experiments. The sinusoidal signal was created by a function generator (BK Precision Model 4078) at a desired forcing frequency f_f and amplitude, delivered to an amplifier (Adcom GFA-7300) with a constant gain of 30 for all forcing conditions in this study.

The jet fluid in the present experiments was comprised of mixtures of He, N_2, and acetone vapor, the latter of which was required for PLIF imaging for separate JICF studies with and without excitation [8,13,16]. Varying the mole fractions of the constituent gases enabled control of the desired mixture density. Mass flow controllers (Tylan Model FC-260) were used to alter the He and N_2 mass flow rates; these species were mixed in a long, cylindrical chamber to passively remove nonuniformities in the gases before entering a temperature-controlled acetone seeder, which maintained the appropriate vapor conditions. The seeded mixture then entered four symmetrically center-oriented injectors beneath the injection/excitation system.

In these studies the jet Reynolds number was kept constant at $\mathrm{Re}_j = 2300$ and the jet-to-crossflow density ratio was fixed at equidensity conditions, $S = 1.00$, while the momentum flux ratio J was independently varied by altering the crossflow velocity U_∞. Prior studies on shear layer instabilities and jet structure for variable density conditions and at different jet Reynolds numbers are documented in Getsinger *et al.* [8]. The specific momentum flux ratios explored in this lock-in study were $J = 61$ and 18, corresponding to a convectively/locally unstable upstream shear layer in the absence of forcing, and $J = 7$, corresponding to a naturally absolutely/globally unstable upstream shear layer [8,14,16]. The free jet in the absence of crossflow, $J \to \infty$, was also examined here. To achieve jet densities equal to that of the crossflow, the jet flow consisted of constituent gases with fixed mole fractions as follows: N_2 ($\psi \approx 0.548$), He ($\psi \approx 0.234$), and acetone ($\psi \approx 0.218$). Jet density and viscosity were determined for these constituents and the relevant flow rates via the Reichenberg method [33].

The present experiments used constant temperature anemometry (CTA) via a single-component, boundary-layer type hotwire probe (Dantec 55P15) to quantify local velocity and shear layer spectral characteristics. The maximum obtainable frequency via CTA was 400 kHz, significantly higher than the Nyquist frequency of 12 kHz, which is twice the maximum applied sinusoidal forcing frequency of 6000 Hz in these experiments. The hotwire was inserted through an opening in the black side wall of the test section and could be traversed in three dimensions with 1 μm accuracy using a triple-axis linearly staged platform. Hotwire data were delivered first to a 90C10 CTA module in a Dantec StreamLine 90N10 frame and then to an AC/DC signal splitter with signal conditioning developed by Hendrickson [34]. The maximum forcing frequency of 6000 Hz resulted from the inherent nonuniform frequency response of the actuation system, consisting of the amplifier, loudspeaker, hotwire, signal conditioner and DAQ board. Rolloff in the signal was pronounced beyond 1000 Hz, and was especially poor above 6000 Hz. Spectral data were fed to a dual channel dynamic signal analyzer (HP Model 35665A) and averaged over 40 instantaneous frequency distributions. The spectral measurements were applied over a 6.4 kHz range, with 8 Hz resolution.

The amplitude of excitation of the perturbed jet was quantified via the hotwire-measured vertical jet velocity, $u_j(t)$, measured at a location 0.2 jet diameters above the center of the jet exit plane. The root-mean square (RMS) of the jet velocity perturbation, $u'_{j,\mathrm{rms}}$, relative to the time-averaged jet velocity at the same location, $\overline{u}_j$, was used to quantify the amplitude of jet excitation:

$$u'_{j,\mathrm{rms}} \equiv \sqrt{\frac{1}{T}\int_{t_1}^{t_1+T}(u_j-\overline{u}_j)^2 dt}, \tag{1}$$

where $T \equiv 1/f_f$ is the period of excitation. The matching of $u'_{j,\mathrm{rms}}$ among different flow and excitation conditions enabled appropriate comparison of the range of jet responses. The RMS values of velocity perturbations explored were in the range $0.008 \leqslant u'_{j,\mathrm{rms}}/U_j \leqslant 0.23$, where the mean jet velocity averaged over the exit plane was $U_j \approx 7.9$ m/s. It is important to note that, because the jet consisted of a mixture of helium, nitrogen, and acetone in these experiments, the hotwire was calibrated in this mixture. As discussed in detail in Shoji [16] and Shoji *et al.* [17], a separate flush round pipe with a known fully-developed laminar velocity distribution at the injector exit in the absence of crossflow was used for this calibration, quantified in the jet Reynolds number range $360 \leqslant \mathrm{Re}_j \leqslant 2800$.

III. RESULTS

A. Lock-in characteristics

To investigate lock-in behavior of the JICF upstream shear layer, a frequency sweep (in input forcing frequency f_f) was applied by the loudspeaker at a fixed amplitude of forcing, $u'_{j,\mathrm{rms}}$, as measured within the USL at a shear layer trajectory location $s/D = 2.0$ (see Figure 1). The general method for determining the critical forcing frequency for lock-in at each $u'_{j,\mathrm{rms}}$ amplitude thus contrasted that used in Davitian *et al.* [11] and Getsinger *et al.* [12], where the frequency f_f is fixed and the amplitude of excitation (pressure perturbation associated with applied excitation) is systematically increased until lock-in is observed in the spectra. The criteria for determining lock-in of the upstream shear layer to f_f were also slightly different in the present study. In previous studies of the transverse jet [11,12] and of the low density free jet [30], lock-in is considered to occur when the USL spectral peak at the unforced natural mode f_o disappears under external forcing, with f_f dominating the spectra. But in the present study, a more precise set of criteria was used: the USL was considered to be locked-in to f_f when sinusoidal forcing caused the amplitude of the fundamental peak at f_o to be reduced by at least three orders of magnitude and, in addition, when there was no evidence of quasiperiodic spectral behavior, as defined in Ref. [31].

For example, USL power spectra for $J = 7$, with a relatively low forcing amplitude corresponding to approximately 1% of the mean jet velocity, matched amongst variable forcing frequencies, are shown in Fig. 3. Note that the $J = 7$ transverse jet creates an absolutely unstable USL in the absence of forcing. In Fig. 3, black lines represent hotwire voltage spectra in the absence of forcing, with a single strong peak at the fundamental frequency $f_o = 2000$ Hz and with higher harmonics at 4000 and 6000 Hz, with very low level disturbances at other frequencies. In this figure, the red lines represent spectra resulting from sine wave forcing for the conditions shown, with a variety of different responses denoted by the spectral peaks. In Fig. 3(a), the forced spectrum shows a strong peak at $f_f = 1200$ Hz and a weaker peak at $f_o = 2000$ Hz, in addition to multiple peaks which in some cases are harmonics of the forcing frequency. Other peaks correspond to frequencies representing linear combinations of the frequencies $|pf_f \pm qf_o|$ (where p and q are integers), representing the interaction between the forcing and natural modes. These forced spectral characteristics in Fig. 3(a) demonstrated quasiperiodicity, similar to observations for the phenomenon in low density free jets, per Li and Juniper [31]. According to the present criteria, $f_f = 1200$ Hz in Fig. 3(a) did not represent a lock-in condition. As forcing frequency increased for the same amplitude, f_f became more dominant in the spectrum, and the peak at f_o lessened as compared with that for the unforced case. In Fig. 3(b) for $f_f = 1400$ Hz, the peak at f_o was reduced

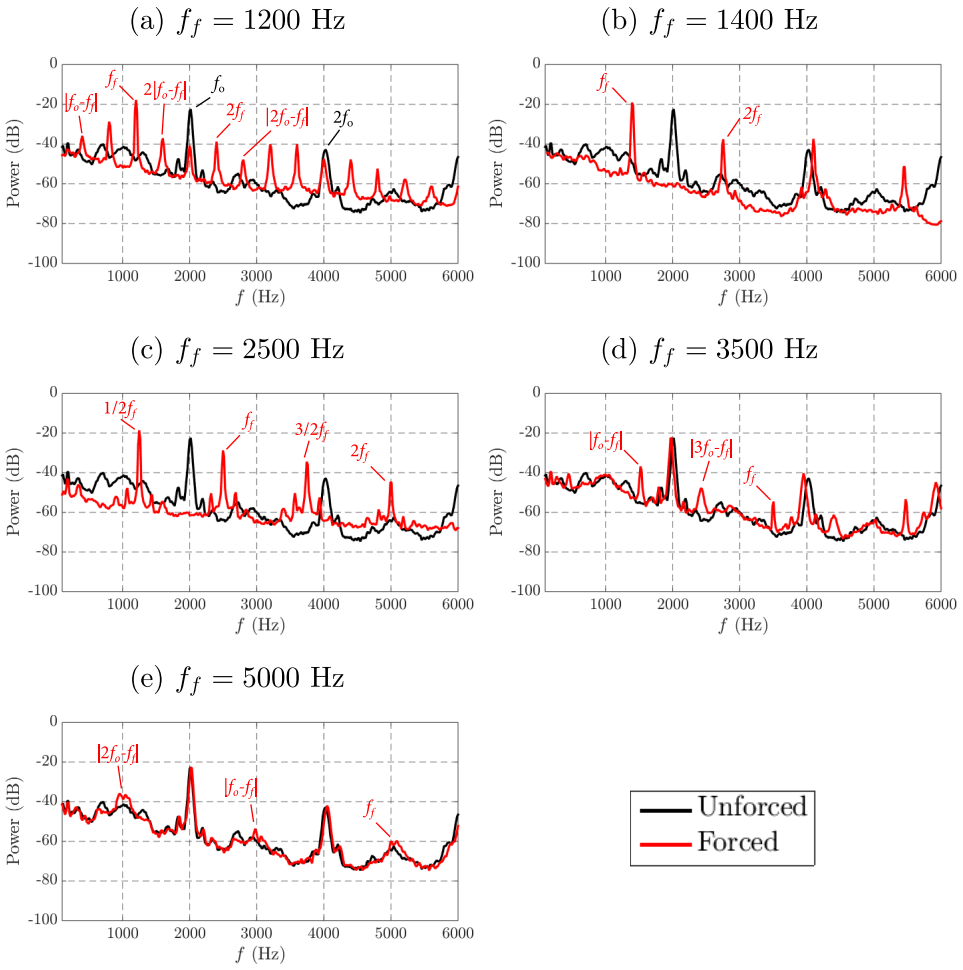

FIG. 3. Power spectra of the hotwire-measured velocity perturbations at the USL trajectory coordinate $s/D = 2.0$ for the JICF at $J = 7$ with/without sinusoidal forcing at forcing frequencies indicated, where $u'_{j,\mathrm{rms}}/U_j \cong 0.01$. The USL had a natural (unforced) USL frequency of $f_o = 2000$ Hz and was considered to be locked-in for conditions shown in panels (b) and (c).

by over 3 orders of magnitude and essentially disappeared; this represented complete dominance of the forcing frequency f_f over the natural mode as well as the disappearance of mode interactions and quasiperiodicity seen at lower frequency forcing. These features provided evidence of a so-called 1:1 lock-in [31]. In Fig. 3(c), forcing at $f_f = 2500$ Hz also led to a significantly diminished peak at f_l with minimal evidence of quasiperiodicity. At higher forcing frequencies ($f_f = 3500$ Hz and 5000 Hz in Figs. 3(d) and 3(e), respectively), in contrast, there was little difference between unforced and forced power spectra, although at $f_f = 3500$ Hz there were a few minor peaks at linear combinations of f_o and f_f, created by the interaction between forcing frequency f_f and the fundamental frequency f_o. These higher forcing frequencies hence were not found to create lock-in.

One can perform the same USL spectral evaluation for other forcing amplitudes and frequencies. Figure 4 shows power spectra for $J = 7$ at a higher forcing amplitude with $u'_{j,\mathrm{rms}}/U_j = 0.08$, matched among variable forcing frequencies. At $f_f = 300$ Hz and 460 Hz [Figs. 4(a) and 4(b)], the interaction between the natural and forcing modes created complicated spectral patterns with spectral peaks at the forcing frequency as well as harmonics of f_f and $|pf_f \pm qf_o|$, again, indicators

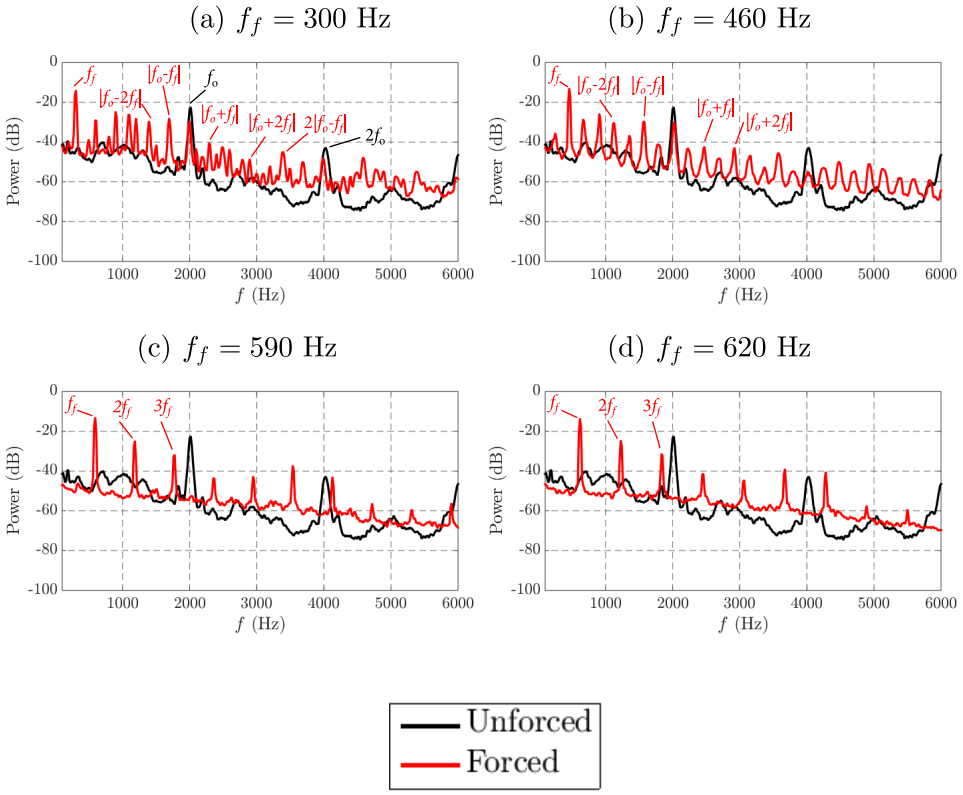

FIG. 4. Power spectra of the hotwire-measured velocity perturbations at the USL trajectory coordinate $s/D = 2.0$ for the JICF at $J = 7$ with/without sinusoidal forcing at forcing frequencies indicated, where $u'_{j,\mathrm{rms}}/U_j = 0.08$. The USL had a natural (unforced) USL frequency of $f_o = 2000$ Hz and was considered to be locked-in above $f_f \approx 590$ Hz [e.g., shown in panels (c) and (d)].

of mode interactions and quasiperiodicity [31]. At $f_f = 590$ Hz [Fig. 4(c)], the spectral peak at the natural frequency f_o virtually completely disappeared and the forcing frequency and its higher harmonics dominated on the USL, corresponding to 1:1 lock-in. The critical minimum forcing frequency for lock-in for the JICF with $J = 7$ at $u'_{j,\mathrm{rms}}/U_j = 0.08$ was determined from data in Fig. 4 as well as additional data [16] to be $f_f \cong 590$ Hz, at least, as f_f was increased toward $f_o = 2000$ Hz. Because the maximum achievable forcing frequency with the current actuation system at $u'_{j,\mathrm{rms}}/U_j = 0.08$ was 1210 Hz (due to a significant roll-off in frequency response above 1000 Hz) [16], lock-in at higher frequencies could not be determined.

Similar determinations of lock-in bands could be made for other forcing amplitudes and frequencies, and for different momentum flux ratios J for the present equidensity studies. Power spectra for $J = 18$, corresponding to the convectively unstable shear layer in the absence of forcing, are shown, for example, in Fig. 5, comparing the unforced spectra with those for sinusoidal excitation at a low forcing amplitude $u'_{j,\mathrm{rms}}/U_j = 0.01$. Without excitation, the black lines in Fig. 5 show multiple weaker peaks around the fundamental at $f_o \approx 2200$ Hz, in addition to higher harmonics and a subharmonic. In general, these multiple frequencies shift slightly and then return to the original values as the hotwire is traversed along the upstream shear layer for CU conditions, as documented extensively in Megerian *et al.* [10]; the frequency shifting is associated with tonal interference between the strengthening shear layer instability and the hotwire probe [12]. Interestingly, with sinusoidal excitation at amplitude $u'_{j,\mathrm{rms}}/U_j = 0.01$, quasiperiodicity in the

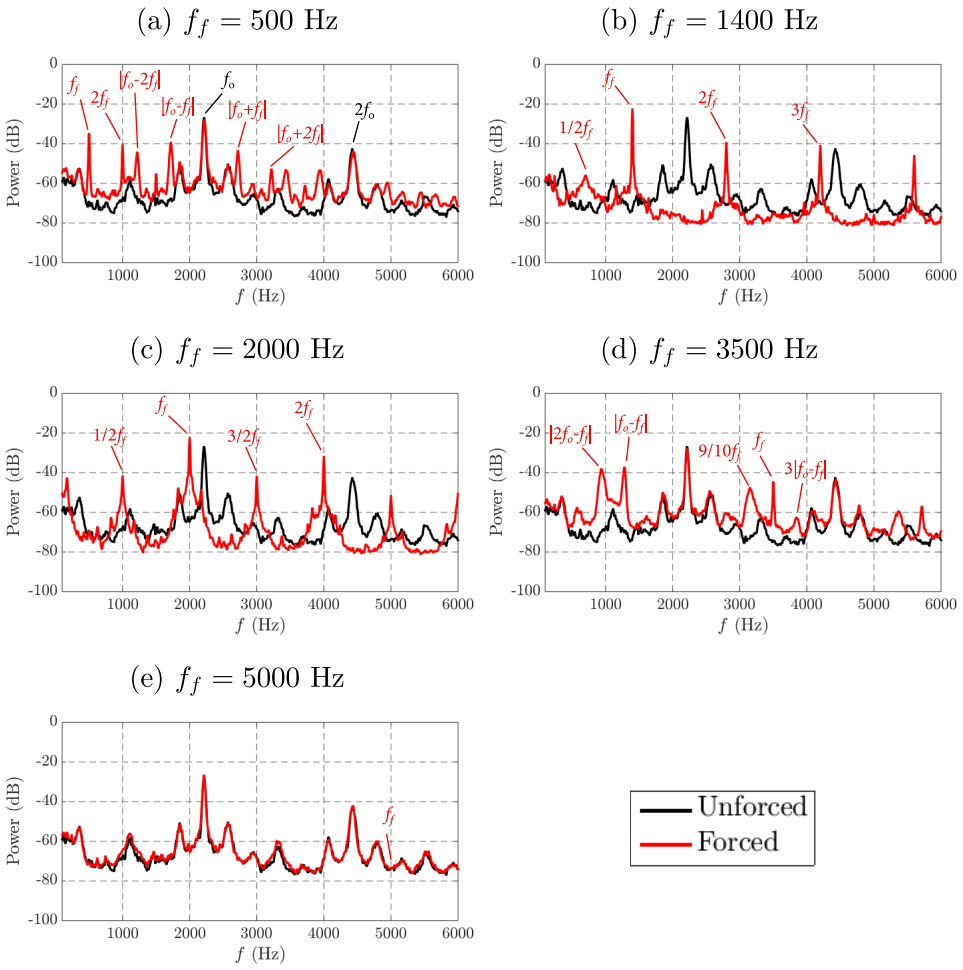

FIG. 5. Power spectra of the hotwire-measured velocity perturbations at the USL trajectory coordinate $s/D = 2.0$ for the JICF at $J = 18$ with/without sinusoidal forcing at forcing frequencies indicated, where $u'_{j,\mathrm{rms}}/U_j = 0.01$. The USL had a natural (unforced) USL frequency of $f_o \approx 2200$ Hz and was considered to be locked-in for conditions shown in panels (b) and (c).

USL was observed in Fig. 5(a) ($f_f = 500$ Hz), suggesting that even the CU USL was not always locked-in to axisymmetric forcing, an unexpected finding based on earlier (less precise) exploration of lock-in for this regime [11]. At $f_f = 1400$ Hz and 2000 Hz (Figs. 5(b) and 5(c), respectively), the fundamental mode disappeared and forcing modes dominated the instability, corresponding to lock-in. But as forcing frequency was increased well above the fundamental mode ($f_o \approx 2200$ Hz), for example, at $f_f = 3500$ Hz and 5000 Hz (Figs. 5(d) and 5(e), respectively), axisymmetric forcing had little to no effect on spectral characteristics, with minor evidence of quasiperiodicity for $f_f = 5000$ Hz. The CU USL responded to axisymmetric forcing similarly to the AU USL despite the fact that the lock-in band was larger in extent for the convectively unstable flow. When excitation of the CU USL was studied for $J = 61$ (Fig. 6), similar trends were observed as those for $J = 18$.

One can apply the same analysis to the shear layer for the free jet injected into quiescent surroundings, which under equidensity conditions is known to be convectively unstable [35,36]. Here power spectra were taken at the shear layer location $s/D = 4.0$ instead of $s/D = 2.0$ because there was no clear peak in the fundamental mode at $s/D = 2.0$, and at that location one could

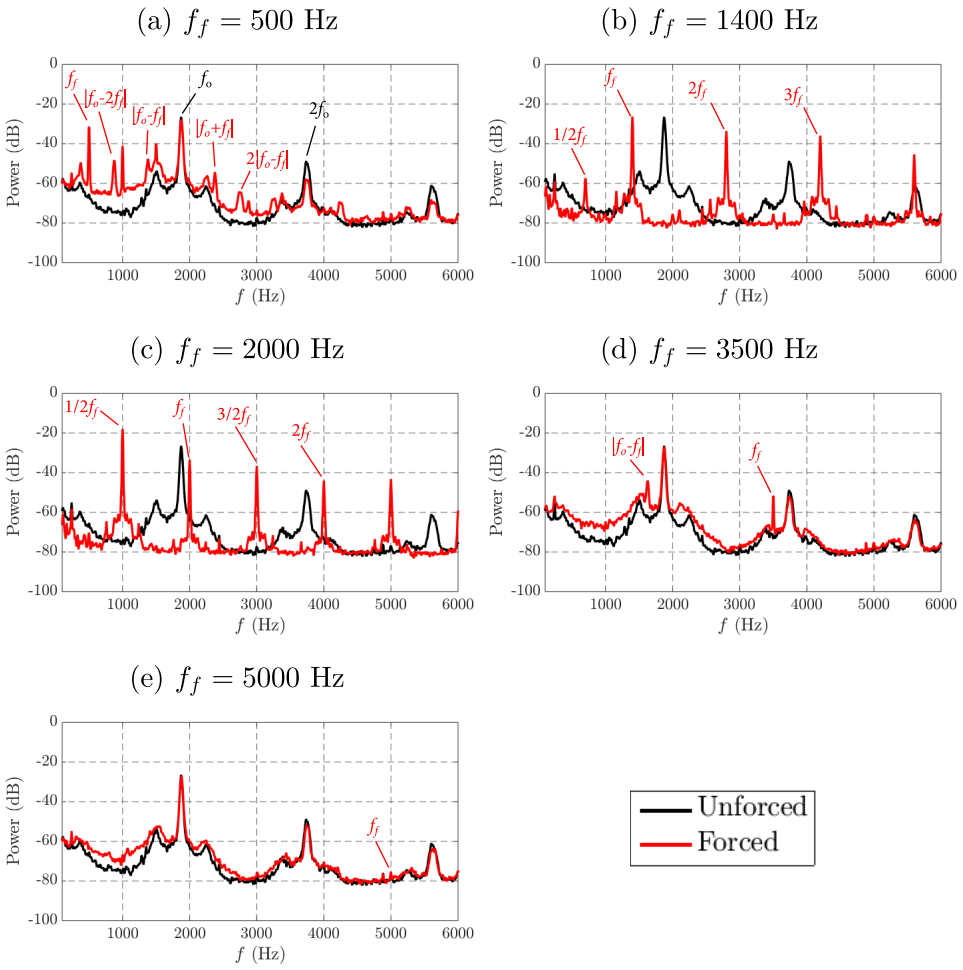

FIG. 6. Power spectra of the hotwire-measured velocity perturbations at the USL trajectory coordinate $s/D = 2.0$ for the JICF at $J = 61$ with/without sinusoidal forcing at forcing frequencies indicated, where $u'_{j,\mathrm{rms}}/U_j = 0.01$. The USL had a natural (unforced) USL frequency in the range $f_o = 1600$–1900 Hz and was considered to be locked-in for conditions shown in panels (b) and (c).

not distinguish whether lock-in occurred. And because the free jet is more susceptible to external forcing than the JICF due to its significantly weaker shear layer instability (with $f_o \approx 1200$ Hz), a forcing amplitude $u'_{j,\mathrm{rms}}/U_j = 0.008$ was applied, the minimum achievable amplitude for the current experimental configuration. Even at a relatively low forcing frequency $f_f = 500$ Hz, as shown for the free jet in Fig. 7(a), the fundamental mode already completely disappeared and the forcing frequencies dominated, clearly indicating shear layer lock-in to f_f. For forcing frequencies lower than 500 Hz, the shear layer was always locked-in. But as forcing frequency was increased, the free jet shear layer continued lock-in behavior until a high enough frequency, e.g., $f_f = 3000$ Hz, was applied [Fig. 7(d)], where the weak fundamental mode was still observed. At higher forcing frequencies, e.g., $f_f = 5000$ Hz [Fig. 7(e)], the shear layer never became locked-in again, and the natural mode was always observed to be dominant over the forcing mode for this amplitude. Remarkably, therefore, the shear layer for the free jet was found to be always locked-in to axisymmetric forcing for $f_f < f_o$ at the minimum forcing amplitude with the current setup, but the shear layer could not achieve lock-in when $f_f \geqslant 3000$ Hz.

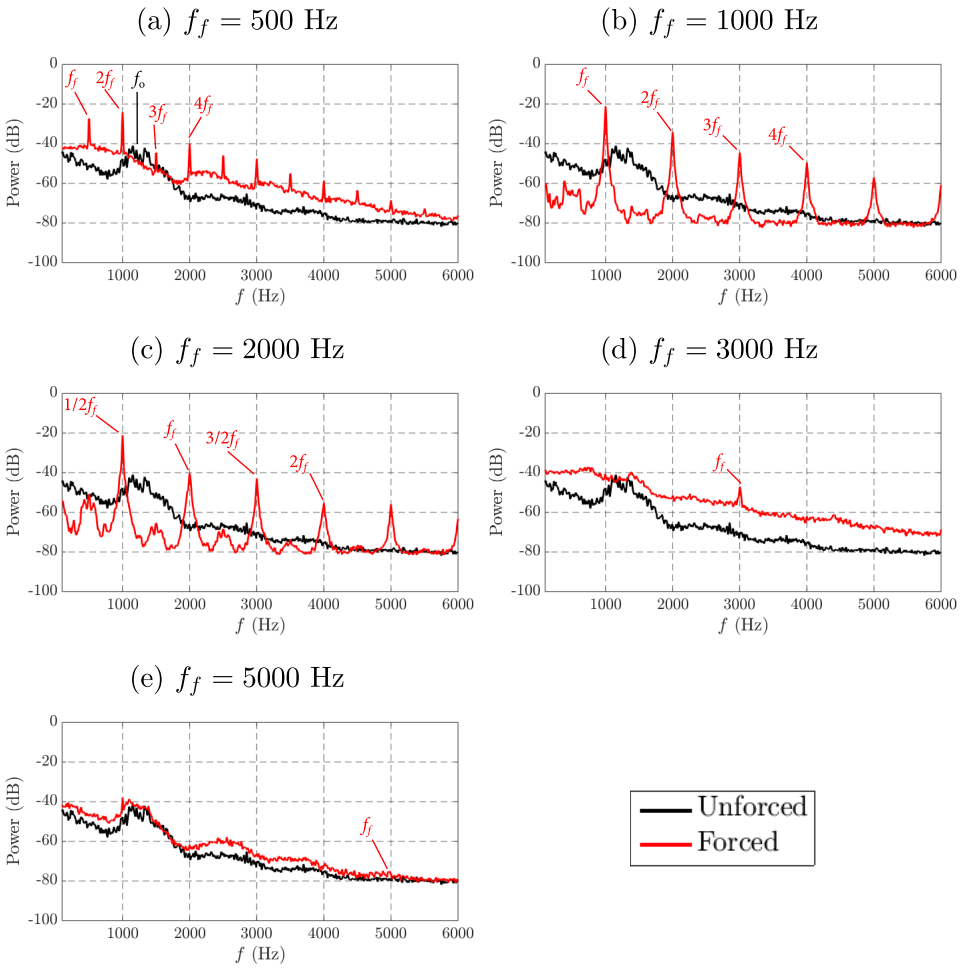

FIG. 7. Power spectra of the hotwire-measured velocity perturbations at the USL trajectory coordinate $s/D = 4.0$ for the free jet with $J \to \infty$ with/without sinusoidal forcing at forcing frequencies indicated, where $u'_{j,\mathrm{rms}}/U_j = 0.008$. The USL had a natural (unforced) USL frequency at $f_o \approx 1200$ Hz and was considered to be locked-in for forcing frequencies $f_f < 3000$ Hz [shown in panels (a)–(c)].

Based on results shown in Figs. 3–7 and in additional datasets, the lock-in diagram can be extracted for a range of J values. Figure 8 shows a lock-in diagram for different J values, that is, the combination of the scaled amplitude $u'_{j,\mathrm{rms}}/U_j$ and scaled critical forcing frequency f_f/f_o producing 1:1 lock-in for JICF conditions $J = 7$, 18, and 61, as well as for the free jet, $J \to \infty$. Prior experimental studies on the transverse jet [11,12] and the low density free jet [30] indicate that the lock-in diagram shows a linear relationship between $|f_f - f_o|$ and the critical acoustic pressure perturbation amplitude in jet forcing, p'_{crit}, suggesting a Hopf bifurcation to a global mode [30,37] and producing a "V" shape in the lock-in diagram involving p'_{crit}. Figure 8 does not show a linear relation between $|f_f - f_o|$ and $u'_{j,\mathrm{rms}}/U_j$, since clearly, $u'_{j,\mathrm{rms}}$ and p'_{crit} do not have a linear relationship, but the figure does produce a minimum at $f_f = f_o$, as expected. As in other studies, Fig. 8 demonstrated that, as forcing frequency approached f_o, or as the amplitude of forcing frequency increased for a given f_f, the forcing could overtake f_o even if the shear layer was naturally absolutely unstable.

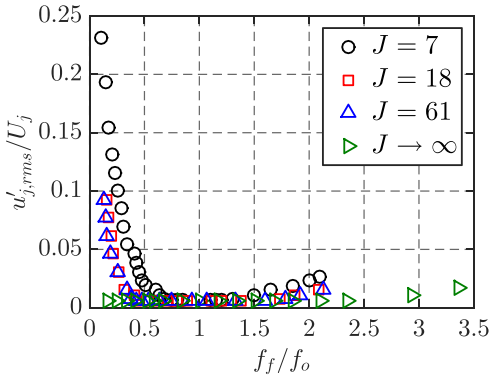

FIG. 8. Lock-in diagrams for the JICF at $J = 7$, 18, and 61, as well as for the free jet, $J \to \infty$, in response to sine wave excitation at various forcing frequencies and scaled amplitudes $u'_{j,\mathrm{rms}}/U_j$, measured at the shear layer locations $s/D = 2.0$ for the transverse jets and $s/D = 4.0$ for the free jet. All symbols represent critical forcing conditions required for 1:1 lock-in of the upstream shear layer to the forcing frequency f_f.

Interestingly, the V-like shape in Fig. 8 displays an asymmetric slope between the lower- and higher-frequency regimes for the transverse jet on either side of $f_f/f_o = 1$, where the slope was much shallower for $f_f > f_o$ than for $f_f < f_o$. This trend suggested that the upstream shear layer was more responsive to external forcing at higher f_f than at lower forcing frequencies. This same orientation in asymmetry is observed for the equidensity JICF (under naturally AU conditions) in earlier studies [11]. But the asymmetry in Fig. 8 was opposite in orientation to the lock-in diagrams in Getsinger *et al.* [12] and Juniper *et al.* [30] for the low density JICF and free jet, respectively, with a shear layer that was more resistant to excitation at higher frequencies ($f_f > f_o$) than at lower frequencies. Clearly, the dynamics of shear layer instabilities and lock-in are different for flows with a variable density than for equidensity conditions, and the influence of crossflow in the transverse jet affects those dynamics.

Observations of quasiperiodicity in the run-up to 1:1 lock-in for the equidensity transverse jet and free jet provided interesting new insights into the complex dynamics of shear layer instabilities. But among the more surprising outcomes of the lock-in study here was the observation that the convectively unstable JICF USL for $J = 18$ and 61 was not always locked-in to external forcing, in contrast to conclusions from more limited datasets for $J = 41$ in Davitian *et al.* [11]. Moreover, the CU free jet shear layer was always found to be locked-in for $f_f < f_o$ in the present studies, but not always locked-in for $f_f > f_o$, a remarkable observation for an equidensity free jet, given that lock-in phenomena for this and other flowfields are more often associated with globally unstable conditions [30–32]. Some of these features may be reminiscent of "marginally" globally unstable flows, which are locally convectively unstable in the entire flowfield but where absolute instability could be incipient at streamwise location(s). These phenomena are discussed in detail by Huerre and Monkewitz [37], Li [38], and Li and Juniper [31].

This lock-in behavior for convectively/locally unstable jet shear layers may be associated with the intrinsic nature of axisymmetric shear layer stability modes and their growth rates in the absence of external forcing. Linear stability analysis (LSA) of the equidensity free jet and transverse jet by Alves *et al.* [39] reveal trends in growth rates for both axisymmetric and helical shear layer stability modes. As indicated in Fig. 7 of Alves *et al.* [39], the free jet's shear layer has a positive axisymmetric growth rate, even at natural frequencies approaching zero, and the growth rates remain positive until a relatively high (but finite) frequency, identical to observations from classical LSA for the equidensity free jet, e.g., per Michalke [40]. This implies that the free jet would require much higher amplitude forcing to achieve a response to excitation at higher frequencies than at lower frequencies, consistent with the ease with which lock-in can be achieved in the latter case.

In contrast, for the equidensity jet in crossflow, the LSA by Alves *et al.* [39] indicates that the upstream shear layer has stable axisymmetric modes at very low frequencies, consistent with greater difficulty to achieve lock-in for this regime (e.g., as shown in Fig. 8). The LSA also indicates positive axisymmetric growth rates that start at a relatively low frequency and remain so until a relatively high but finite natural frequency which decreases with decreasing J or R, that is, for frequencies below that for the free jet. These axisymmetric growth rate trends are also qualitatively consistent with transverse jet lock-in observations at higher frequencies in Fig. 8. While not conclusive, the unexpected trends in lock-in phenomena here were generally consistent with linear stability analysis trends for axisymmetric modes of the transverse jet and the free jet, and bear more extensive exploration.

B. Poincaré maps

Additional evidence and insights may be found for transverse jet and free jet shear layer lock-in via nonlinear time-series analysis, which can be a useful tool for studying dynamical features of physical systems whose intrinsic dynamics are governed by nonlinear processes [41]. In the present study on the JICF, one can reconstruct the phase space for various conditions using state variables extracted from experimental time-series data. In the typical phase space, the state variable of a dynamical system at a given instant of time appears as a single point, while multiple points of the state variable as time $t \to \infty$ create a trajectory in the phase space, with topological features which can be interpreted in terms of dynamical characteristics of the system. For example, as described in Li and Juniper [31] for the low density free jet, although the phase space cannot be directly measured, it can be reconstructed from experimentally (or computationally) extracted temporal data using time-delay embedding [42], since many measurable state variables are intrinsically coupled to one another. The present study applied time-delay embedding to the measured temporally variable hotwire voltage, V_{hw}, acquired at the USL trajectory coordinate $s/D = 2.0$ to characterize the dynamics of the JICF USL with and without axisymmetric sinusoidal forcing for $J = 7$ and 61, corresponding to naturally absolutely/globally and convectively/locally unstable upstream shear layers in the absence of external forcing, respectively. Note that local fluctuations in the acetone mole fraction made it difficult to correlate the temporally varying hotwire voltage directly to vertical jet velocity along the USL, although the hotwire voltage itself contains the same frequency and spectral content as velocity, as confirmed separately [16]. The optimal time delay parameter τ, required for time-delay embedding, was chosen to be the first zero-crossing of the autocorrelation function applied to the temporal hotwire voltage, consistent with the methods in Li and Juniper [31,32].

To extract dynamical characteristics of the JICF, we utilized a two-dimensional section through the three-dimensional phase space [31,32]. The two-dimensional section consisted of a one-way intersection of the phase space trajectory with the plane $V_{\mathrm{hw}}(t - 2\tau) = 0^{+}$, called a "one-sided" Poincaré map. Per Strogatz [43] and Balanov *et al.* [44], for example, in a Poincaré map, a periodic limit cycle appears as a point, while a quasiperiodic oscillation with two incommensurate modes appears as a continuous ring or a two-dimensional torus. Based on these topological features, one can extract nonlinear dynamical characteristics of the unforced and forced JICF. The Poincaré map analysis will be relevant to van der Pol oscillator modeling for the flowfield, described in Sec. III C.

Figure 9 represents Poincaré maps [$V_{\mathrm{hw}}(t - \tau)$ versus $V_{\mathrm{hw}}(t)$] for $J = 7$, at a matched forcing amplitude of $u'_{j,\mathrm{rms}}/U_j = 0.01$ for a range of frequencies f_f. In the absence of forcing, in Fig. 9(a), the Poincaré map shows a small blob, which is a typical topological characteristic for the global instability as extracted from experimental data points. A global instability (or a periodic limit cycle) ideally would show a single data point for temporal data without any noise [44], but with experimental noise, a blob would be present. With increasing forcing frequency, from $f_f = 1200$ Hz to 2500 Hz [Figs. 9(b)–9(d)], the blob became gradually smaller, suggesting stronger periodicity caused by the lock-in of the USL to f_f. It should be noted that, at $f_f = 1200$ Hz, the shape of the blob in Fig. 9(b) became smaller than for the unforced case but was less circular, with a

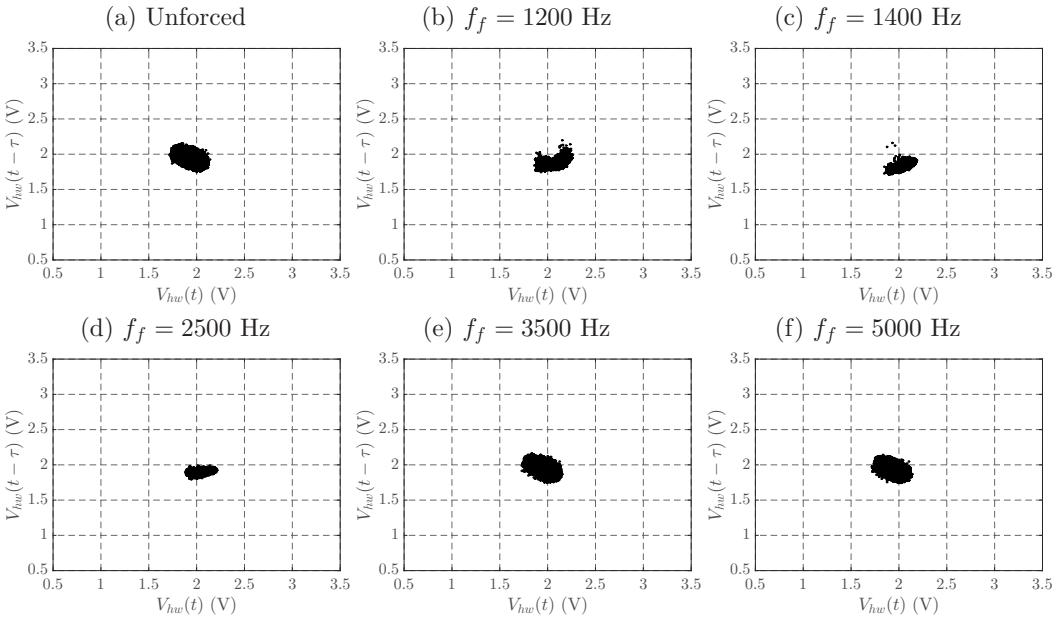

FIG. 9. Poincaré maps of the hotwire voltage at the USL trajectory coordinate $s/D = 2.0$ for the JICF at $J = 7$ with/without sinusoidal forcing at forcing frequencies as indicated, for forcing amplitude $u'_{j,\mathrm{rms}}/U_j \cong 0.01$ (cf. Fig. 3). The USL was considered locked-in for forcing conditions shown in panels (c) and (d), and quasiperiodic for conditions in panels (b) and (e).

cusp-like structure, suggesting that there was a slight propensity for the initiation of quasiperiodicity. The Poincaré map in Fig. 9(b) appeared to be consistent with the quasiperiodicity observed in spectra corresponding to this excitation condition [Fig. 3(a)]. And when the USL was forced fairly close to the fundamental frequency $f_o = 2000$ Hz, e.g., $f_f = 1400$ Hz [Fig. 9(c)] and 2500 Hz [Fig. 9(d)], the Poincaré map became smaller in size than for the unforced case, consistent with spectral lock-in behavior as documented in Figs. 3(b) and 3(c), respectively. As forcing frequency was increased further, to 3500 Hz [Fig. 9(e)] and 5000 Hz [Fig. 9(f)], at which the USL spectra were nearly identical to the unforced USL [Figs. 3(d) and 3(e), respectively], Poincaré maps were topologically nearly identical to those for the unforced case [Fig. 9(a)]. Hence, the Poincaré maps here showed very good consistency with the spectral-based categorization of USL instability response to axisymmetric forcing.

Poincaré maps also can be created for other flow conditions, e.g., for $J = 7$ at a higher forcing amplitude of $u'_{j,\mathrm{rms}}/U_j = 0.08$ (Fig. 10) and for $J = 61$ at an amplitude of $u'_{j,\mathrm{rms}}/U_j = 0.01$ (Fig. 11). At $J = 7$ at this higher forcing amplitude, when the USL was not locked-in at $f_f = 300$ Hz [Fig. 10(b)], the Poincaré map showed a slightly larger blob shape than for unforced conditions, generally consistent with a periodic limit cycle. But at a higher forcing frequency in the run-up to lock-in [at $f_f = 460$ Hz, in Fig. 10(c)], a torus-like shape appeared in the Poincaré map. Per Li and Juniper [31] and Kashinath *et al.* [45], the creation of a torus-like shape can be labeled a "torus-birth bifurcation," a topological characteristic indicating the transition from periodicity (for the naturally occurring instability) to quasiperiodicity. Such quasiperiodicity was indeed observed in power spectra under the forcing conditions in Fig. 10(c), as shown in Fig. 4(b). Then once the USL became locked-in, as defined for higher frequency forcing via the spectra in Figs. 4(c) and 4(d), the corresponding Poincaré maps [Figs. 10(d) and 10(e), respectively] returned to smaller blob shapes, although the slight cusp observed at $f_f = 590$ Hz reflected the additional peaks and a transition from quasiperiodicity observed in the spectra.

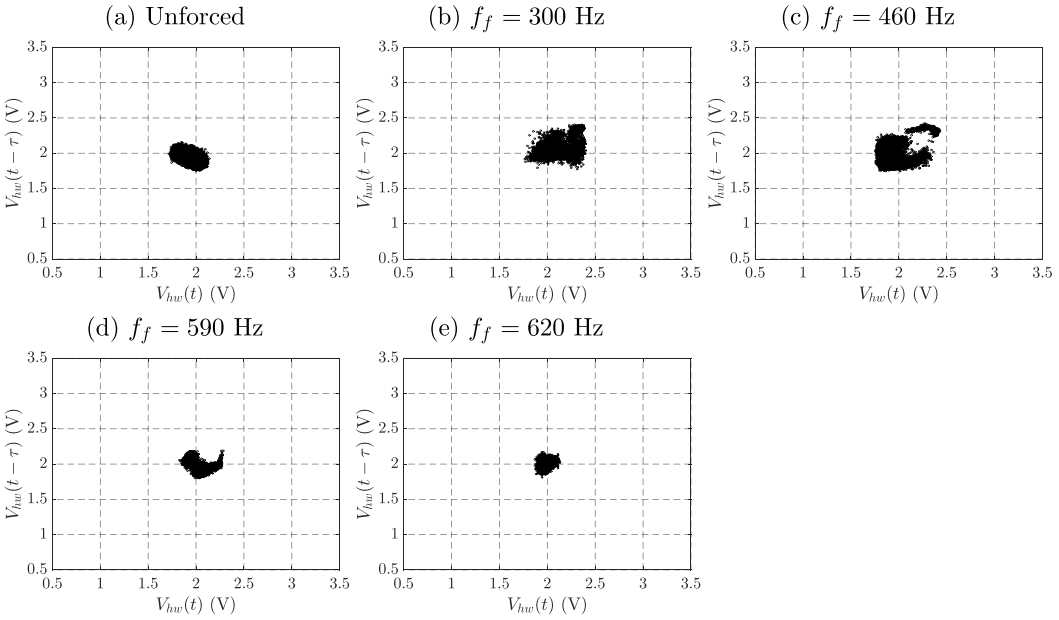

FIG. 10. Poincaré maps of the hotwire voltage at the USL trajectory coordinate $s/D = 2.0$ for the JICF at $J = 7$ with/without sinusoidal forcing at forcing frequencies as indicated, for forcing amplitude $u'_{j,\mathrm{rms}}/U_j = 0.08$ (cf. Fig. 4). The USL was considered locked-in for forcing conditions shown in panels (d) and (e) and quasiperiodic for conditions in panels (b) and (c).

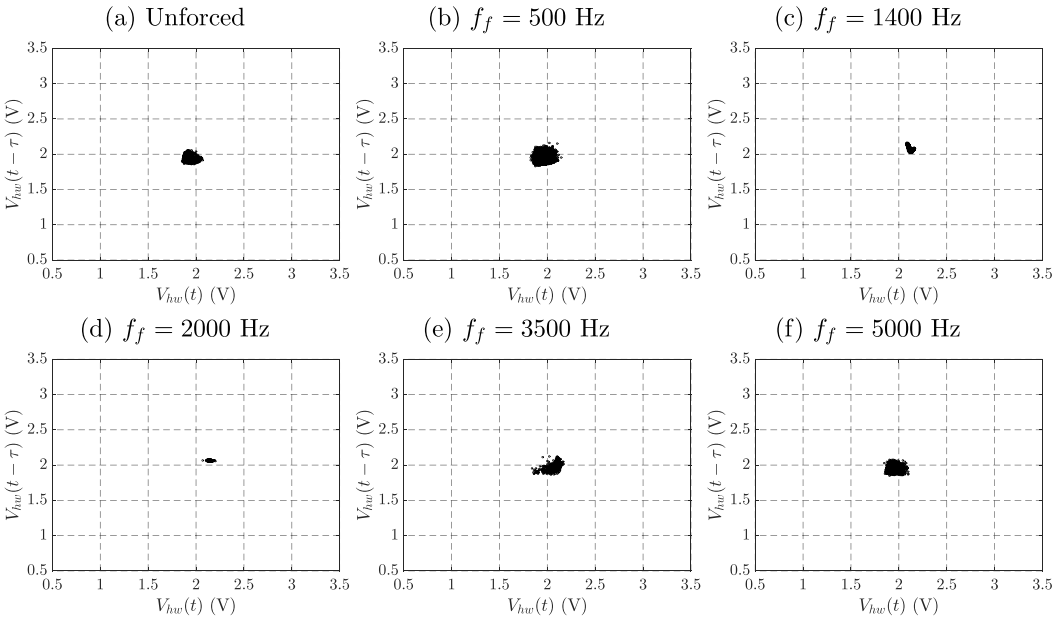

FIG. 11. Poincaré maps of the hotwire voltage at the USL trajectory coordinate $s/D = 2.0$ for the JICF at $J = 61$ with/without sinusoidal forcing at forcing frequencies as indicated, for forcing amplitude $u'_{j,\mathrm{rms}}/U_j = 0.01$ (cf. Fig. 6). The USL was considered locked-in for forcing conditions shown in panels (c) and (d), and quasiperiodic for conditions in panels (b) and (e).

In Fig. 11 for the $J = 61$ case, which in the absence of forcing had a convectively unstable USL, Poincaré maps showed a blob which became smaller as forcing frequency increased to approach the fundamental frequency range of $f_o = 1600$–1900 Hz [Figs. 11(c) and 11(d)]. While spectra at $f_f = 500$ Hz [Fig. 6(a)] showed relatively weak quasiperiodicity, the corresponding Poincaré map in Fig. 11(a) did not produce clear topological features for quasiperiodicity, such as a torus structure, likely due to the fairly low forcing amplitude used here, as also seen in the $J = 7$ results in Fig. 9.

C. van der Pol oscillator model

The van der Pol (VDP) oscillator is a well-known second-order ordinary differential equation (ODE) capable of representing self-excited dynamical systems [46]. The VDP oscillator model has been successfully applied to represent the forcing response of a number of flowfields, including the reactive/nonreactive free jet in quiescent surroundings [31,32,45]. This particular oscillator is a fairly simple nonlinear model for self-excited flow systems, and is able to replicate trends in experimental data and hence to capture essential dynamical features. In the present study on the equidensity JICF, the VDP model was used to model self-excited upstream shear layer dynamics for the $J = 7$ case with and without sinusoidal excitation at a relatively strong forcing amplitude corresponding to $u_{j,\mathrm{rms}}/U_j = 0.08$. A range of forcing frequencies was explored, with the aim of having the model approximate the measured temporal hotwire voltage variation, power spectra (Fig. 4), and Poincaré map (Fig. 10) for the $J = 7$ condition.

With an external sinusoidal forcing source term as in the present experiments, the general VDP oscillator model can be formulated as follows:

$$\ddot{z} - \epsilon(1 - z^2)\dot{z} + \omega_o^2 z = B\sin(\omega_f t), \tag{2}$$

where z is the dynamical variable in question and ω_o is the natural angular frequency of the dynamical system. The forcing term on the right-hand side of Eq. (2) represents external, sinusoidal excitation of a system with forcing amplitude B and a forcing frequency ω_f, while the feedback parameter, ϵ, controls the degree of linear self-excitation and nonlinear self-limitation of the system. In the present study, following the same procedure as for the low density free jet in Li and Juniper [31], the feedback parameter ϵ was specifically chosen to be a fixed value of 0.41, corresponding to a matching of the lock-in frequency extracted from this model to the experimentally observed value ($f_f/f_o \approx 0.295$). The selection of $\epsilon = 0.41$ also represented lock-in and quasiperiodic dynamical characteristics of the self-excited JICF with forcing at $u'_{j,\mathrm{rms}}/U_j = 0.08$ quite well, as will be shown.

The second-order ODE in Eq. (2) was solved using a multiple variable-order algorithm [47]; the procedure followed that in Li and Juniper [31], and details on this approach may be found in that study. Note that, in the absence of external forcing in Eq. (2), i.e., $B = 0$, the system modeled by the VDP oscillation contains a weak nonlinearity with a perfectly circular phase trajectory in the phase space for $\epsilon \ll 1$, while the system contains a strong nonlinearity without a circular phase trajectory for $\epsilon \gg 1$. Yet a dynamical system for either condition converges to a stable limit cycle, regardless of initial conditions, due to its intrinsic behavior as a periodic attractor of the VDP oscillator. The natural angular frequency ω_o was set to 1 for relative scaling of all conditions, although of course the actual natural frequency was not necessarily 1 because of intrinsic nonlinearities when $\epsilon > 0$. As done for the experimental data (see Sec. III B), a two-dimensional section, or "one-sided" Poincaré map through the three-dimensional phase space, was again utilized in extracting the dynamical maps.

Figure 12 shows power spectra [Figs. 12(a)–12(c)] and Poincaré maps [Figs. 12(d)–12(f)] extracted from the temporal results of the VDP model with $\epsilon = 0.41$, corresponding to data for the experimental case of $J = 7$ with forcing amplitude $u'_{j,\mathrm{rms}}/U_j = 0.08$. Here the forcing amplitude parameter B was selected to be 0 for the unforced case and 1.13 for the forced cases, the latter of which was chosen to produce good qualitative agreement between the model and experiments for a fixed forcing amplitude at a range of different frequencies, per the approach in Li and Juniper [31]. For the unforced case [Figs. 12(a) and 12(d)], consistent with an absolutely unstable USL with

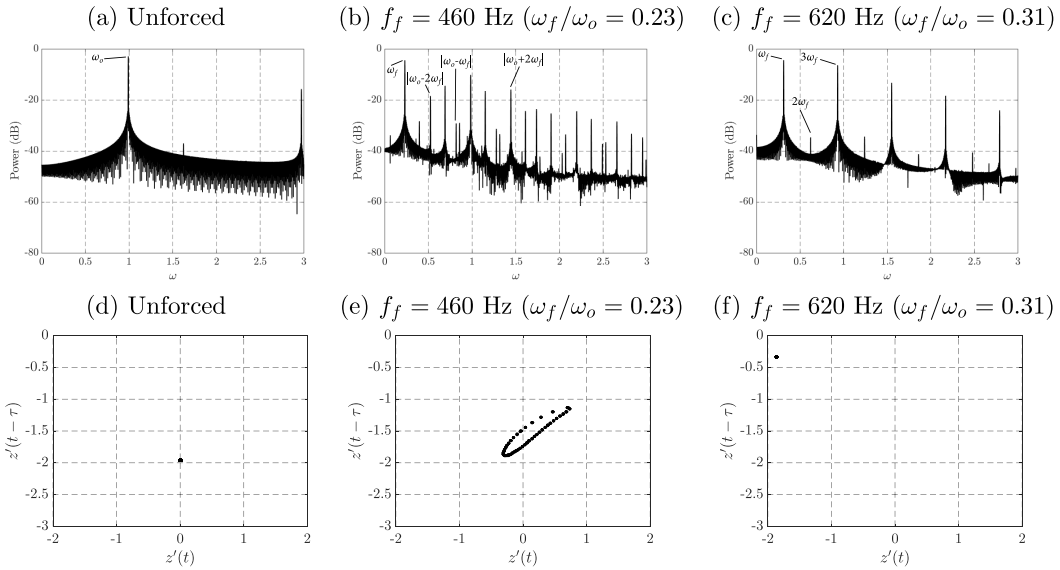

FIG. 12. VDP oscillator model results representing spectral dynamics (a)–(c) and Poincaré maps (d)–(f) corresponding to the USL trajectory coordinate $s/D = 2.0$ for the JICF at $J = 7$ with/without sinusoidal forcing at an amplitude equivalent to $u'_{j,\mathrm{rms}}/U_j = 0.08$. The USL had a natural (unforced) USL frequency of $f_o = 2000$ Hz, corresponding to $\omega_o = 1$, and was considered to be locked-in via experiments for $f_f > 590$ Hz, shown in panels (c) and (f).

strong natural periodicity, power spectra showed a strong peak at the fundamental frequency ω_o, and the Poincaré map reduced to a single data point (i.e., the theoretical limit of an infinitely small blob), consistent with a periodic limit cycle. At forcing frequency $f_f = 460$ Hz, corresponding to $\omega_f/\omega_o \approx 0.23$ in the VDP model, the solution produced multiple peaks, at forcing frequency ω_f and at frequencies $|p\omega_f \pm q\omega_o|$, where p and q are integers, in the predicted power spectra [Fig. 12(b)]. Correspondingly, there was a torus-like structure predicted in the Poincaré map [Fig. 12(e)]. These characteristics suggested quasiperiodicity at this forcing condition due to the interaction between natural modes of the instability and the forcing mode, consistent with experimental observations for this condition [Fig. 4(b) for the spectra and Fig. 10(c) for the Poincaré map]. For a higher forcing frequency of $f_f = 620$ Hz ($\omega_f/\omega_o \approx 0.31$ in the VDP model), at which the USL for $J = 7$ was locked-in for the experiments, per Fig. 4(d), the peak in the spectrum at the naturally occurring fundamental frequency completely disappeared, and the forcing frequency and its higher harmonics dominated the power spectra, shown in Fig. 12(c). This strong periodicity produced a single data point in the Poincaré map [Fig. 12(f)], as expected for 1:1 lock-in, with general consistency with the experimental data [Fig. 10(e)]. Overall, the instability characteristics from these model results for power spectra and topological features in Poincaré maps were qualitatively consistent with results from experiments for the $J = 7$, $u'_{j,\mathrm{rms}}/U_j = 0.08$ conditions in Figs. 4 and 10. The simple VDP model for this transverse jet condition not only replicated the dynamics of lock-in and quasiperiodicity, but also provided additional evidence that the unforced condition for the transverse jet at a low momentum flux ratio demonstrated self-excitation, consistent with long-standing observations in earlier transverse jet experiments [8,10,11].

IV. DISCUSSION AND CONCLUSIONS

This largely experimental study explored the dynamical characteristics of the equidensity transverse jet, with a special focus on lock-in and quasiperiodicity generated via axisymmetric

sinusoidal jet forcing for different jet-to-crossflow momentum flux ratios J, spanning conditions producing both naturally occurring convectively and absolutely unstable upstream shear layers. For the JICF with an absolutely/globally unstable USL in the absence of external excitation ($J = 7$), as observed in other AU/GU flows, power spectra showed that the USL can be made to lock-in to sinusoidal forcing at a large enough amplitude, with virtually complete disappearance of its natural mode f_o and dominance of a forcing mode f_f. For certain forcing amplitudes, lock-in as well as quasiperiodicity, as the lock-in band was approached, were observed in upstream shear layer spectra. These phenomena were also visible in Poincaré maps extracted from the experimental measurements, with the so-called "torus-birth" structure consistent with quasiperiodicity. The results in this low momentum flux ratio ($J = 7$) regime were consistent with predictions of shear layer dynamics from a Van der Pol (VDP) oscillator model, which demonstrated clear global instability behavior without sinusoidal forcing and quasiperiodicity and lock-in for specific forcing conditions. For the JICF with a naturally AU/GU USL, these findings provide additional evidence for consistency with upstream shear layer self-excitation. Indeed, the VDP modeling also demonstrates that lock-in and quasiperiodic dynamics observed for the JICF are not restricted to this specific flow system, but are generic features of forced self-excited oscillators.

An unexpected finding in the present studies occurred for JICF flow conditions for which a convectively/locally unstable upstream shear layer formed in the absence of external forcing (here, momentum flux ratios $J = 18$ and 61). In the present experiments with sinusoidal jet excitation, the USL was not always observed to be locked-in to applied sinusoidal forcing, in contrast to prior limited experimental conditions explored by Davitian *et al.* [11] and in contrast to the typical expectation of straightforward lock-in for a weakly unstable shear layer. As indicated in Fig. 8, lock-in bands for these convectively unstable conditions were nearly identical to one another, and were broader in frequency range than that for the JICF with a globally unstable shear layer at $J = 7$. Remarkably, even the equidensity free jet ($J \to \infty$) with a CU shear layer demonstrated lock-in behavior in the higher forcing frequency range, but not at low forcing frequencies. These findings on lock-in for CU flows were in fact consistent with theoretically determined axisymmetric growth rates for transverse jet shear layer instabilities observed in the linear stability analysis of Alves *et al.* [39], where positive growth rates for instabilities within specific frequency ranges suggest that lock-in bounds should exist for convectively unstable flow conditions. Quasiperiodicity in the run-up to lock-in was also observed in the present study for the convectively unstable USL, not only via spectral characteristics but also in experimentally-derived Poincaré maps.

The evidence for complex dynamics associated with sinusoidal excitation of the equidensity transverse jet is not only interesting and consistent with the VDP dynamical model for a self-excited flow, but it also suggests that the control of JICF behavior via external forcing could have differing effects on jet behavior. The implications for jet structure and mixing when the upstream shear layer is locked-in as opposed to quasiperiodic or only weakly affected by external forcing are subject of several alternative excitation modalities currently under exploration.

ACKNOWLEDGMENTS

The authors express their thanks to Prof. Leonardo Alves of the Universidade Federal Fluminense (UFF) and to Prof. Matthew Juniper of the University of Cambridge for helpful discussions on this study. This project has been supported by the National Science Foundation under Grant No. CBET-1437014 and by the Air Force Office of Scientific Research under Grant No. FA9550-15-1-0261.

[1] R. J. Margason, Fifty years of jet in cross flow research, *AGARD Conference Proceedings*, AGARD-CP-534 (1993).

[2] A. R. Karagozian, Transverse jets and their control, Prog. Energy Combust. Sci. **36**, 531 (2010).

[3] K. Mahesh, The interaction of jets with crossflow, Annu. Rev. Fluid Mech. **45**, 379 (2013).

[4] Y. Kamotani and I. Greber, Experiments on a turbulent jet in a cross flow, AIAA J. **10**, 1425 (1972).
[5] A. R. Karagozian, An analytical model for the vorticity associated with a transverse jet, AIAA J. **24**, 429 (1986).
[6] R. M. Kelso, T. T. Lim, and A. E. Perry, An experimental study of round jets in cross-flow, J. Fluid Mech. **306**, 111 (1996).
[7] L. Cortelezzi and A. R. Karagozian, On the formation of the counter-rotating vortex pair in transverse jets, J. Fluid Mech. **446**, 347 (2001).
[8] D. R. Getsinger, L. Gevorkyan, O. I. Smith, and A. R. Karagozian, Structural and stablity characteristics of jets in crossflow, J. Fluid Mech. **760**, 342 (2014).
[9] T. F. Fric and A. Roshko, Vortical structure in the wake of a transverse jet, J. Fluid Mech. **279**, 1 (1994).
[10] S. Megerian, J. Davitian, L. S. de B. Alves, and A. R. Karagozian, Transverse-jet shear-layer instabilities. part 1. experimental studies, J. Fluid Mech. **593**, 93 (2007).
[11] J. Davitian, D. Getsinger, C. Hendrickson, and A. R. Karagozian, Transition to global instability in transverse-jet shear layers, J. Fluid Mech. **661**, 294 (2010).
[12] D. R. Getsinger, C. Hendrickson, and A. R. Karagozian, Shear layer instabilities in low-density transverse jets, Exp. Fluids **53**, 783 (2012).
[13] L. Gevorkyan, T. Shoji, D. R. Getsinger, O. I. Smith, and A. R. Karagozian, Transverse jet mixing characteristics, J. Fluid Mech. **790**, 237 (2016).
[14] L. Gevorkyan, T. Shoji, W. Y. Peng, and A. R. Karagozian, Influence of the velocity field on scalar transport in gaseous transverse jets, J. Fluid Mech. **834**, 173 (2018).
[15] P. S. Iyer and K. Mahesh, A numerical study of shear layer characteristics of low-speed transverse jets, J. Fluid Mech. **790**, 275 (2016).
[16] T. Shoji, Mixing and Structural Characteristics of Unforced and Forced Jets in Crossflow, Ph.D. thesis, University of California, Los Angeles 2017.
[17] T. Shoji, A. Besnard, E. W. Harris, R. T. M'Closkey, and A. R. Karagozian, Effects of axisymmetric square wave excitation on transverse jet structure and mixing, AIAA J. **57**, 5 (2019).
[18] S. C. Crow and F. H. Champagne, Orderly structure in jet turbulence, J. Fluid Mech. **48**, 547 (1971).
[19] R. T. M'Closkey, J. King, L. Cortelezzi, and A. R. Karagozian, The actively controlled jet in crossflow, J. Fluid Mech. **452**, 325 (2002).
[20] S. Narayanan, P. Barooah, and J. M. Cohen, Dynamics and control of an isolated jet in crossflow, AIAA J. **41**, 2316 (2003).
[21] H. Johari, Scaling of fully pulsed jets in crossflow, AIAA J. **44**, 2719 (2006).
[22] J. Davitian, C. Hendrickson, D. Getsinger, R. T. M'Closkey, and A. R. Karagozian, Strategic control of transverse jet shear layer instabilities, AIAA J. **48**, 2145 (2010).
[23] R. E. D. Bishop and A. Y. Hassan, The lift and drag forces on a circular cylinder in a flowing fluid, Proc. R. Soc. London Series **277**, 51 (1964).
[24] G. H. Koopmann, The vortex wakes of vibrating cylinders at low Reynolds numbers, J. Fluid Mech. **28**, 501 (1967).
[25] P. K. Stansby, The locking-on of vortex shedding due to the cross-stream vibration of circular cylinders in uniform and shear flows, J. Fluid Mech. **74**, 641 (1976).
[26] D. J. Olinger and K. R. Sreenivasan, Nonlinear Dynamics of the Wake of an Oscillating Cylinder, Phys. Rev. Lett. **60**, 797 (1988).
[27] R. D. Blevins, *Flow-Induced Vibration*, 2nd ed. (Krieger Publishing Company, Malabar, FL, 1990).
[28] H. Schlichting and K. Gersten, *Boundary Layer Theory*, 8th ed. (Springer, Berlin, 1999).
[29] X. Yang and A. Zebib, Absolute and convective instability of a cylinder wake, Phys. Fluid A: Fluid Dynamics **1**, 689 (1989).
[30] M. P. Juniper, L. K. B. Li, and J. W. Nichols, Forcing of self-excited round jet diffusion flames, Proc. Combust. Inst. **32**, 1191 (2009).
[31] L. K. B. Li and M. P. Juniper, Lock-in and quasiperiodicity in a forced hydrodynamically self-excited jet, J. Fluid Mech. **726**, 624 (2013).
[32] L. K. B. Li and M. P. Juniper, Lock-in and quasiperiodicity in hydrodynamically self-excited flames: Experiments and modeling, Proc. Combust. Inst. **34**, 947 (2013).

[33] B. E. Poling, J. M. Prausnitz, and J. P. O'Connell, *The Properties of Gases and Liquids*, 5th ed. (McGraw-Hill, New York, 2001).
[34] C. S. Hendrickson, Identification and Control of the Jet in Crossflow, Ph.D. thesis, University of California, Los Angeles 2012.
[35] P. J. Strykowski and D. L. Niccum, The influence of velocity and density ratio on the dynamics of spatially developing mixing layers, Phys. Fluids A **4**, 770 (1992).
[36] M. P. Hallberg and P. J. Strykowski, On the universality of global modes in low-density axisymmetric jets, J. Fluid Mech. **569**, 493 (2006).
[37] P. Huerre and P. A. Monkewitz, Local and global instabilities in spatially developing flows, Annu. Rev. Fluid Mech. **22**, 473 (1990).
[38] L. K. B. Li, Forcing of globally unstable jets and flames, Ph.D. thesis, University of Cambridge 2011.
[39] L. S. de B. Alves, R. E. Kelly, and A. R. Karagozian, Transverse-jet shear-layer instabilities. part 2. linear analysis for large jet-to-crossflow velocity ratio, J. Fluid Mech. **602**, 383 (2008).
[40] A. Michalke, Survey on jet instability theory, Progr. Aerospace Sci. **21**, 159 (1984).
[41] H. Kantz and T. Schreiber, *Nonlinear Time Series Analysis*, 2nd ed. (Cambridge University Press, Cambridge, 2003).
[42] F. Takens, Detecting strange attractors in turbulence, in *Dynamical Systems and Turbulence*, Vol. 898, edited by D. A. Rand and L. S. Young (Springer, Berlin, 1981), pp. 366–381.
[43] S. H. Strogatz, *Nonlinear Dynamics and Chaos with Applications to Physics, Biology, Chemistry, and Engineering* (Perseus Books, Reading, MA, 1994).
[44] A. Balanov, N. Janson N, D. Postnov, and O. Sosnovtseva, 1:1 forced synchronization of periodic oscillations, in *Synchronization: From Simple to Complex. Springer Series in Synergetics.* (Springer, Berlin/Heidelberg, 2009), pp. 21–73.
[45] K. Kashinath, L. K. B. Li, and M. P. Juniper, Forced synchronization of periodic and aperiodic thermoacoustic oscillations: lock-in, bifurcations and open-loop control, J. Fluid Mech. **838**, 690 (2018).
[46] B. van der Pol and J. van der Mark, Frequency demultiplication, Nature **120**, 363 (1927).
[47] L. F. Shampine and M. W. Reichelt, The matlab ode suite, SIAM J. Sci. Comput. **18**, 1 (1997).